

HUMAP: Hierarchical Uniform Manifold Approximation and Projection

Wilson E. Marcílio-Jr, Danilo M. Eler, Fernando V. Paulovich, Member, IEEE, Rafael M. Martins, Member, IEEE

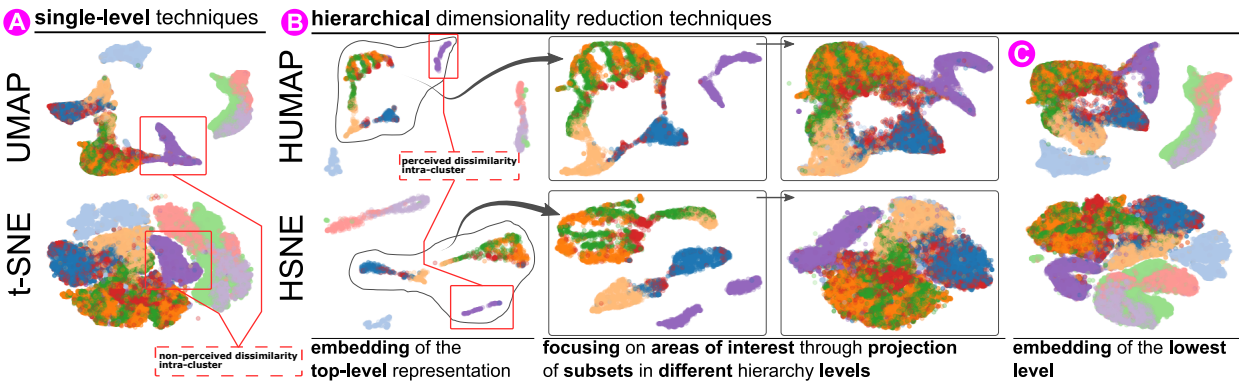


Fig. 1: Comparison of traditional dimensionality reduction (DR) techniques (A) vs. hierarchical DR techniques (B). Traditional techniques operate at a single level of detail and focus on delivering a big picture that depicts the dataset as a whole, ignoring fine-grained details of intra-cluster distributions and making it difficult to proceed with more detailed investigations. On the other hand, hierarchical DR (HDR) approaches summarize important intra-cluster information already in the top-level representations of the hierarchy imposed on the input data without affecting the layout's overall organization. Our hierarchical approach, called HUMAP, extends HDR techniques state of the art by preserving the mental map when requesting more details about clusters while balancing the trade-off between global and local relations. This characteristic is apparent in the first three layouts for hierarchical DR results (B). For HUMAP, the projected data subsets in different hierarchy levels resemble superior hierarchy levels, while users receive more information about the similarity among clusters. Furthermore, HUMAP also preserves the mental map of different hierarchy levels; the top-level representation (B) resembles the lowest-level representation (C).

Abstract— Dimensionality reduction (DR) techniques help analysts understand patterns in high-dimensional spaces. These techniques, often represented by scatter plots, are employed in diverse science domains and facilitate similarity analysis among clusters and data samples. For datasets containing many granularities or when analysis follows the information visualization mantra, hierarchical DR techniques are the most suitable approach since they present major structures beforehand and details on demand. However, current hierarchical DR techniques are not fully capable of addressing literature problems because they do not preserve the projection mental map across hierarchical levels or are not suitable for most data types. This work presents HUMAP, a novel hierarchical dimensionality reduction technique designed to be flexible in preserving local and global structures and the mental map throughout hierarchical exploration. We provide empirical evidence of our technique's superiority compared with current hierarchical approaches and show two case studies to demonstrate its strengths.

Index Terms— Dimensionality reduction, hierarchical exploration.

1 INTRODUCTION

The majority of knowledge domains now require high-dimensional data analysis as a fundamental task. However, the challenge of new applications comes with the expansion of high-dimensional data availability. Dimension reduction (DR) is one of the most notable examples of how visualization tools for analysis and navigation are becoming more and more crucial in these situations. DR techniques generally aim to decrease the dimensionality of a dataset while maintaining the structure present in the initial high-dimensional space [32]. The analysis of

document collections [7], gene expression data [14, 20, 39, 43, 44], and features learned by deep learning models [4, 36] are just a few tasks supported by DR results (or embeddings), which are represented as scatter plots. Practitioners typically search for DR techniques for these applications that can reveal complex structures (like manifolds), preserve clusters, and offer accurate representations of the global relationship among clusters.

Traditionally, DR techniques operate at a single level of detail, resulting in layouts that emphasize general patterns that convey the overall distribution of points in the high-dimensional space. These layouts, however, might conceal crucial data characteristics, such as dissimilarities in sample characteristics within a cluster, that would give a summary of the structures and benefit analysis when focusing on critical information first. To solve this problem, one could always create a new projection using a cluster of interest or a subset of data instances, but the resulting layout would not take into account the contribution of the other points, and context would not be preserved. With the aid of hierarchical DR (HDR) techniques, which encourage the exploration of DR outcomes using the maxim of visual information-seeking [42]: *Overview first, zoom and filter, then details-on-demand*.

- W. E. Marcílio-Jr and D. M. Eler are with São Paulo State University (UNESP), Brazil. E-mails: {wilson.marcilio, danilo.eler} @unesp.br.
- F. V. Paulovich is with Eindhoven University of Technology, the Netherlands. E-mail: f.paulovich@tue.nl
- R. M. Martins is with Linnaeus University, Växjö, Sweden E-mail: rafael.martins@lnu.se

Manuscript received xx xxx. 201x; accepted xx xxx. 201x. Date of Publication xx xxx. 201x; date of current version xx xxx. 201x. For information on obtaining reprints of this article, please send e-mail to: reprints@ieee.org. Digital Object Identifier: xx.xxxx/TVCG.201x.xxxxxx

In HDR, the detailed structures seen in traditional representations are summarized, but groups inside clusters are better encoded. Users expand clusters in the HDR representations to investigate lower (and more detailed) hierarchy levels discovering the relationship the subclusters that are more visible on top-level representation. Fig. 1 illustrates well this idea for the class in purple that is also highlighted by a red box. Using HDR approaches, the separation of two dominant structures (the purple clusters highlighted by a red box in Fig. 1(B)) is visible for the top-level representations, which is not true for traditional approaches. Then, an aspect brought by our approach is the mental-map preservation for maintaining the context throughout hierarchical exploration. This is important due to the various non-linear transformations that happens to the data after an embedding step, as illustrated for HSNE in Fig. 1(B) for the second and third embeddings. Notice that the positioning and structural relations among clusters are lost during layout optimization, making it necessary to maintain the mental map—especially for unlabelled datasets.

Although groups inside clusters are better encoded in HDR, the detailed structures seen in conventional representations are summarized. By examining lower (and more detailed) hierarchy levels through expanding clusters in HDR representations, users can learn more about the relationships between the subclusters that are more obvious on the top-level representation. This concept is well-illustrated for the class in purple on Fig. 1, which is also given extra emphasis by a red box. Traditional approaches do not allow for the top-level representations to show the separation of two dominant structures (the purple clusters highlighted by a red box in Fig. 1(B)). The preservation of mental maps is another component of our strategy for preserving context during hierarchical exploration. This is crucial because the data undergoes numerous non-linear transformations following an embedding step, as shown for HSNE in Fig. 1(B) for the second and third embeddings. Keep in mind that positioning and structural relationships between clusters are lost during layout optimization, necessitating the maintenance of the mental map, particularly for unlabeled datasets.

Although HDR has been a focus of research for the past few years, the methods currently available have some drawbacks [13, 21, 35]. HiPP [33] uses nodes, which are circles with varying size, to provide a summary of the dataset and direct users toward additional analysis. Least Square Projection (LSP) [34], on which it is based, does not scale well for large numbers of data points. Using a GPU implementation, HSNE [35] can successfully represent manifolds and manage tens of thousands of data points and dimensions. However, HSNE does not maintain the user’s mental map as the analyst drills down the hierarchy. In other words, the embedding generated for a hierarchical level does not take the previous level into account, and as the hierarchy is expanded, the results typically diverge more and more from the embeddings of the previous level. Such a characteristic of the HSNE embeddings is depicted in Fig. 1 (B, bottom). Lately, a hierarchical method called Multiscale PHATE [21] was proposed to function with mass cytometry data. The technique appears to struggle with much higher dimensions or when the dataset lacks a continuous characteristic, despite being able to handle large datasets with continuous phenomena. Furthermore, Multiscale PHATE has very limited interaction options because when users drill down into the hierarchy, they can only select from the clusters defined during hierarchy definition.

The preservation of the mental map across hierarchy levels and maintaining a good trade-off between the preservation of global and local structures in the low-dimensional representation of the dataset are two HDR design considerations that these techniques cannot fully address. From the perspective of local and global preservation, some hierarchical approaches (such as HiPP) struggle to fully uncover complex manifold structures or have trouble doing so depending on the type of dataset. For instance, Multiscale PHATE excels at separating clusters when the goal is continuous or evolutionary datasets. Last but not least, methods to reveal complex structures while maintaining the global and local relationships among data samples are currently needed. When analyzing deep learning models [27, 36] and gene expression data [25], for instance, it is essential to find a compromise between the preservation of global and local relations. These quality standards

are provided by HSNE for higher hierarchical levels. However, users are unable to switch between overview and details because it does not preserve the mental map as the hierarchy is expanded.

To meet these challenges, we present Hierarchical Uniform Manifold Approximation and Projection (HUMAP). Our HDR technique, which is based on UMAP [28], creates a hierarchy on the dataset by encoding both global and local similarity information between data points in a two-step similarity definition. HUMAP successfully reveals complex structures present in the numerous granularities of a dataset while maintaining the mental map as the user drills down the hierarchy by using projected data points from higher levels to influence the low-dimensional representation of lower hierarchy levels. We provide experimental evidence that HUMAP addresses the aforementioned design considerations through visual and quantitative evaluation. We also offer two in-depth case studies that examine the characteristics of a deep learning model and the hierarchical justification of DR outcomes. In summary, the contribution of this paper is a novel HDR technique¹ that improves the representation of both global and local relations while preserving the mental map across hierarchy levels.

The remainder of this paper is organized as follows. Section 2 presents the related works. We describe our technique in Section 3 and present a case study in Section 4. In Section 5 we quantitatively evaluate HUMAP and compare it against state-of-the-art HDR techniques. Discussions are presented in Section 6 and in Section 7 we draw our conclusions.

2 RELATED WORK

By reducing the number of dimensions while maintaining structural and similarity relations in the low-dimensional representation, DR techniques aid in the analysis of high-dimensional datasets [32]. Users typically search for patterns in the data when using a DR technique, such as clusters, shapes, and outliers. To ensure a successful data exploration process, it is essential to understand the data and the available DR techniques. For instance, linear DR techniques are well known for quickly revealing variability [17, 18, 34]. While generally being more difficult and time-consuming, non-linear DR techniques [26, 28, 29, 35] can reveal more complex structures that are present in high-dimensional space.

The scatterplot metaphor is frequently employed represent DR results. Despite being widely used for exploratory data analysis [Micallef 2017], scatter plots lack effectiveness due to marker overlap [40, 41]. When exploring large datasets as a whole, traditional DR techniques may obscure crucial details within and between clusters. For instance, some datasets exhibit inherently multilevel structures [25], which call for a DR technique to be more adaptable. Knowledge discovery is facilitated in this way by strategies that make exploration simpler and direct users through the exploratory process. One such strategy is the use of hierarchical dimensionality reduction (HDR) techniques, which offer exploration mechanisms based on the mantra *overview first & details-on-demand* [42], concentrating on essential information as needed by the user.

There are many traditional DR strategies (see [8, 32] for helpful surveys), but very few hierarchical DR (HDR) methods [13, 32]. These HDR methods have the feature of first establishing the hierarchical structure before enabling multilevel exploration. The challenge is conveying different levels while preserving context and neighborhood structures [32]. Therefore, current studies concentrate on defining the hierarchical structure while using the projection engine of previous traditional DR approaches. For example, in order to solve the MDS computational complexity problem, MDSteer [46] incrementally computes a multidimensional scaling layout in response to user demand. Glimmer [15] also addresses MDS complexity by performing projection using a multilevel GPU scheme. Simply put, the authors interpolate high hierarchy levels to create a hierarchy. However, MDS-based approaches do not adequately capture the complex structures (such as manifolds) found in the majority of real-world and practical datasets (e.g., deep learning features, image collections, or biological data).

¹<https://github.com/wilsonjr/humap>

Hierarchical PCA variants suffer from a lack of non-linear structure communication strategies [1, 16, 45].

Data organization in HiPP [33] involves landmarks and hierarchical clustering. In finer levels, the data points are represented and influenced by the landmarks of coarser levels. HiPP uses a force algorithm to deal with overlaps when positioning points heuristically and takes into account the landmarks of LSP [34] for context preservation and to communicate hierarchy levels. One of the most reliable methods is HSNE [35]. The HSNE algorithm builds a hierarchy to preserve global and local relationships at high hierarchy levels using random walks on a transition matrix. The analysis is hampered when mental map preservation is crucial because the HSNE's embeddings lose the structural relationships that were presented at higher levels during hierarchical exploration. To provide interactive analysis in a reasonable amount of time, HSNE also needs a GPU. Using diffusion condensation [5], a recent method known as Multiscale PHATE [21] computes a manifold-intrinsic diffusion space on the input data and condenses data points towards centroids to produce groups of multiple granularities. Massive datasets can be handled by multiscale PHATE, but only for a few dimensions. Additionally, it appears to have issues with its embedding engine when the input dataset does not contain continuous phenomena [30]. The hierarchy levels of these methods all share the inclusion of representative samples or landmarks. It is interesting to note that any single-level-of-detail dimensionality reduction method that projects data points onto landmarks is capable of having a hierarchical version [32].

Finally, users essentially work with embeddings of various data subsets of increasing size during hierarchical exploration. Thus, it is essential to maintain the mental map between successive projections in order to prevent users from being tricked by geometrical transformations during exploratory data analysis. When examining deep learning features, the preservation of the mental map in DR layouts—often referred to as *projection alignment*—has drawn attention [6, 37]. A time-varying dataset is projected using dynamic t-SNE [37] to reduce temporal variability that is unimportant to the final layout. This is accomplished by including a term in the cost equation for the t-SNE that regulates the trade-off between alignment and conventional t-SNE optimization. A trade-off parameter is also used in VFF (Hilasaca 2020) to regulate the alignment of projections in feature fusion tasks. VFF [12], however, is ineffective for preserving local structures [6]. Finally, Cantareira and Paulovich [6] proposed a general model for projection alignment that incorporates the original cost function of the DR technique and a penalty term applied for alignment. In contrast to these methods, our approach to maintaining the mental map entails directing the movement of data samples that have already been projected at high hierarchy levels and affecting the placement of new data samples.

To address the issues with previous techniques, we present HUMAP. Our method offers a tunable parameter to maintain the mental map across hierarchy levels and during drill-down operations, and it is very flexible for preserving both local and global relations. Fig. 1 illustrates these characteristics. The highest hierarchy level (top-level) of HUMAP resembles the lowest hierarchy level and maintains the structures of chosen subsets (B). In contrast to single-level techniques (A), it summarizes the data while providing information on the connections between and within clusters.

3 HIERARCHICAL UNIFORM MANIFOLD APPROXIMATION AND PROJECTION (HUMAP)

Two main components of our HDR technique are *Hierarchy construction* and *Projection* (Fig. 2). In the former, we use a similarity measure between landmarks to create a tree-like structure on the high-dimensional dataset. In the latter, we incorporate the hierarchy levels in response to the user's demand for more specific data. All the steps (A–G) in this process are shown in Fig. 2.

The first step in building a hierarchy from bottom to top is to use a kernel function to determine the connection strengths (local affinities) of a k -nearest neighbor graph of data points in the high-dimensional space \mathbb{R}^m (step A). Then, similar to previous research [35], we employ the Finite Markov Chain (FMC) to identify the most visited nodes,

which consist of the landmarks for the higher level (step C). Steps (D) and (E) of the FMC process are used to encode local and global neighborhood information for each landmark as well as to build a neighborhood structure for high hierarchy levels (> 1). In order to define a new hierarchy level, a new neighborhood graph is created in step (F) using the computed similarity (step G).

For projecting hierarchy levels, the neighborhood graph is first symmetrized (step H), so each edge's strength helps in finding a suitable position in the low-dimensional representation. For the purpose of maintaining mental maps, the projection of lower levels, with the exception of the top hierarchy level, is influenced by the low-dimensional positions (I) of data points in higher levels, which we discuss in Section 3.3.2.

We use a few strategies from UMAP [28] to build our approach, including the kernel function to calculate the connection strengths among data samples and the embedding strategy and concepts from HSNE [35] for landmark selection. We concentrate on the HUMAP components for hierarchical dimensionality reduction in the following section.

3.1 Landmark selection

DR methods frequently use k -nearest neighbor graphs to capture manifolds in high-dimensional spaces. The path formed by the vertices in the k -nearest neighbor graph is used to represent the distance between two arbitrary points in the high-dimensional space in this process, which approximates global distances by adding up local relations [29]. Therefore, the first step in many DR techniques that can find manifolds in data is to fit a k -nearest neighbor graph [26, 28, 29].

After finding the k -nearest neighbor graph, a kernel function defines the strength (or probability) of every edge in the graph. Here, we adopted UMAP's [28] kernel function for two data points $x_i, x_j \in X$ (the high-dimensional dataset):

$$p_{i|j} = e^{-\frac{d(x_i, x_j) - \rho_i}{\sigma_i}} \quad (1)$$

where $d(x_i, x_j)$ is the euclidean distance between the data points x_i and x_j , ρ_i is the euclidean distance of x_i to its closest neighbor, and σ_i is a kernel value that depends on the number of neighbors k , according to the following equation [28],

$$k = 2^{\sum_i p_{i|j}}. \quad (2)$$

Notice that σ_i is unknown. However, by fixing a value for k , we can use Equation 2 to compute it using a binary search [28]. That is, for each data point x_i (matrix row), Equation 1 is plugged into Equation 2 and a binary search is used to find the best σ_i value given the number of nearest neighbors (k). Thus, the value for σ_i that produces a k' closest to the actual k is selected. This procedure ensures a different kernel value (σ_i) for each data point and its neighborhood. For a fixed k , higher σ_i values encode dense neighborhoods while lower σ_i values encode sparse neighborhoods. In other words, σ_i encodes how close the data points are in the neighborhood of x_i . Lastly, the parameter ρ_i gives a locally adaptive kernel for each data point and ensures a good topological representation of high-dimensional data [28].

The connection strength between each neighbor is determined by computing $p_{i|j}$ for each pair of data points in accordance with the neighborhood density (please, see Equation 1). The dataset is summarized at higher hierarchical levels using good representative data points (or landmarks) based on the strengths of these connections. For this task, we use random walks on a finite markov chain, as in Pezzotti et al.'s [35] work (FMC). The path from an initial state to the final state after μ steps (or hops) on the neighborhood graph is known as a random walk and is defined by a length. As a result, we compute the following equation to generate the transition probabilities for the FMC from $p_{i|j}$:

$$T_{i,j} = \frac{p_{i|j}}{\sum_k p_{i|k}} \quad (j, k \in NH(i)), \quad (3)$$

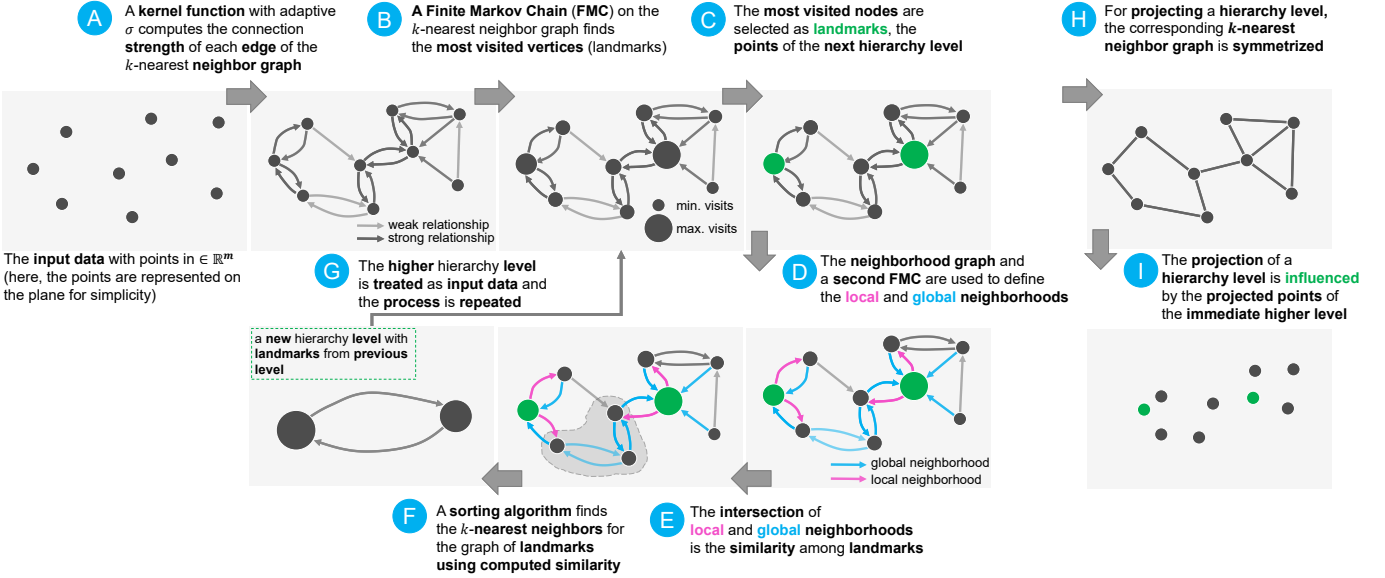


Fig. 2: The hierarchy is built from the bottom up. First, the connection strength between data points in the high-dimensional space is determined using a k -nearest neighbor graph and a kernel function (A). After several random walk steps, the graph’s structure and the strength of the connections are used to determine which nodes have been visited the most (B). The landmarks, or most frequented nodes in the graph, correspond to the points in the higher hierarchy level (C). To repeat the same procedure for high hierarchy levels, we calculate the intersection of representation neighborhoods (E), which were formed by joining local and global neighborhoods, to determine how similar two landmarks are (D). With the exception of the first hierarchy level (all data), we compute the k -nearest neighbors using a sorting algorithm (F). We employ a modified UMAP (McInnes 2018) optimization for projecting hierarchy levels (or subsets of them). We initialize the low-dimensional representation by fixing the coordinates already computed for higher hierarchy levels, even though the projection (H) requires a symmetrized version of the k -nearest neighbor graph (I).

where data points x_j and x_k are in the neighborhood of x_i ($NH(i)$). Then, the landmarks are sampled from $T_{i,j}$ by a simple Markov Chain Monte Carlo technique [11]. For each data point i , we start n random walks with length μ . We empirically evaluated that $n = \mu = 10$ results in embeddings that trustfully represent the underlying data structure. This whole process, from kernel smoothing to landmark selection, is represented by the steps from (A) to (C) in Fig. 2.

Unlike previous approaches [21, 35], users have control over the number of data points in each hierarchy level, making it easier to experiment with datasets with varying characteristics (e.g., cluster density)—though other threshold-based approaches can be used [35]. By specifying the number of landmarks on level i ($|H^i|$), users control the number of data points in a hierarchy level. We store the random walk endpoints and choose the $|H^i|$ most frequented data points as landmarks during the Monte Carlo simulation.

3.2 Dissimilarity definition

When building the hierarchy, the hierarchical level H^i encodes information of the level below (H^{i-1}). This ensures that the information at the top-level accurately represents the information in the whole dataset. Therefore, for each subsequent hierarchy level, we transfer the manifold and structure relationships from bottom to top. For the first hierarchical level, the similarity between two data points x_i and x_j is computed using Equation 1 based on euclidean distance ($d(x_i, x_j)$), as in Fig. 2 (A). For higher levels, the similarities among landmarks in H^i follow the data organization of H^{i-1} . Such similarities are computed based on the k -nearest neighbor graph of H^{i-1} .

On level i , for two landmarks, l_u^i and l_v^i , we compute their similarity using two components: the intersection of the global and local neighborhoods. Fig. 2 (D-F) illustrates these two components for two landmarks in green. The local neighborhood (in pink) consists of the k -nearest neighbors as usual, while the global neighborhood (computed only for $H^i, i \leq 1$) is found through random walks (in blue). Two landmarks that share more local neighbors are very close in the high-dimensional space

since there are single data points that connect them (for landmarks (l_u^i) and (l_v^i), there is a data point (l_p^i) in the neighborhood of (l_u^i) and (l_v^i)). Landmarks sharing global neighbors have global relationships since there is a path between these landmarks. In Fig. 2, the landmarks in green only share a global relationship, highlighted in gray between steps (E) and (F).

We use random walks to compute the global neighborhood (the blue relationship in Fig. 2) similarly to the HSNE [35] approach. In this case, we start ω random walks of length ν from each non-landmark (x_k^{i-1}) on the k -nearest neighbor graph of H^{i-1} . Then, when a random walk reaches a landmark, (l_u^i), we add the non-landmark (x_k^{i-1}) to the “representation neighborhood” of landmark l_u^i . Notice that such a representation neighborhood (RNH) is created only for similarity computation.

The local neighborhood component adapts our approach to preserve more of the local structures (see the pink relationship in Fig. 2). To this end, we use the k -nearest neighbors (NH) of each landmark l_u^i to augment their representation neighborhoods with the $\beta \times |NH(l_u^i)|$ first nearest neighbors of l_u^i , where β is a threshold between 0 and 1. Thus, the greater β , the more important the k -nearest neighbors, and the similarity measure will encode more local relations. HUMAP supports parameter tuning to perform better on neighborhood preservation. The similarity between two landmarks consists of the intersection between their global and local neighborhoods. The local neighborhood for a landmark is in the set of its nearest neighbors, so one can increase it by adjusting the parameter $\beta \in [0, 1]$ that adds $\beta|NH(i)|$ neighbors to the local neighborhood—by default, β is set to 0. We evaluated HUMAP with different values of β and found a clear relationship between local neighborhoods and neighborhood preservation.

Finding these two components results in the representation neighborhood (RNH) for each landmark l_u^i on level H^i . Such a neighborhood consists of a sparse matrix RNH of dimensions $|H^i| \times |H^{i-1}|$ where $RNH_{u,v}$ is 1 if $x_v^{i-1} \in RNH(l_u^i)$ or 0, otherwise. The similarity among

landmarks is computed based on the intersection of representation neighborhoods, that is, the shaded area of Fig. 2 (E-F). We compute the intersection with the RNH matrices as follows:

$$d_{RNH}(l_u^i, l_v^i) = \frac{(RNH_u)^T RNH_v}{M}, \quad (4)$$

$$M = \max_n \left(\sum_{n=1}^{|L^{i-1}|} RNH_{m,n} \right)$$

where M is a normalization factor that ensures similarity between 0 and 1—notice that since RNH is sparse, computing the above matrix multiplication is fast in practice. Note that the intersection between neighborhoods is also used in HSNE to compute the similarity between two landmarks. However, unlike in HSNE, we do not directly employ such a similarity measure to compute the embeddings. Instead, HUMAP extends the neighborhood to encode global information and uses UMAP's kernel to maintain its properties throughout the hierarchy.

The output of the above operation is a similarity measure, meaning that a value equal to 1 corresponds to landmarks sharing the same representation neighborhood, as illustrated by the operation (F) in Fig. 2. Thus, we transform it into a dissimilarity measure by subtracting the similarity value from 1. To benefit from UMAP's kernel function (Equation 1), this process of creating the neighborhood using Markov Chain also eliminates the necessity to perform another kNN step. Using the dissimilarity, we can simply apply the same kernel function on every hierarchical level.

3.3 Generating the embedding

Having the dissimilarity values $(1 - D_{RNH})$, where D_{RNH} is a matrix with d_{RNH} as rows, we are able to use them in Equation 1 to generate the matrix p_{ij} for each hierarchical level. Then, HUMAP, as in UMAP [28] technique, applies the following matrix symmetrization to produce an undirected weighted graph:

$$p_{ij} = p_{i|j} + p_{p|j} - p_{i|j}p_{j|i}. \quad (5)$$

The matrix p_{ij} is used to produce an embedding that converges to positions in a low-dimensional space. While we refer to McInnes et al. [28] for a detailed description of the UMAP algorithm, it is important to mention that an initial low-dimensional representation of the dataset is created using Spectral Embedding [31]. Then, p_{ij} is used to reposition the data points using a force-directed graph layout whose convergence is performed by decreasing attractive and repulsive forces (given by p_{ij}) using Stochastic Gradient Descent [38].

3.3.1 Subset projection

Each landmark represents a set of data points on the level below when hierarchical levels are defined. It is crucial to specify the functionality of interaction with hierarchical levels and request more detail (more data points) of a data subset in order to keep track of such representation.

Each non-landmark data point on level H^{i-1} is linked up with a landmark on level H^i in two steps. The first step entails going through the landmarks iteratively and designating which of their neighbors will be influenced by them. A landmark will eventually attempt to "represent" a data point that has already been represented. As a result, we designate the data point as being a part of the area surrounding the closest landmark. The majority of data points are assigned to a landmark by this process, but it is still necessary to look for instances where data points are not in any landmark's neighborhood. In this case, we iterate over each data point on H^{i-1} to make sure that it is not associated with a landmark in case we want to search its neighborhood. This procedure is described in detail in Algorithm 1. We examine the neighborhood of each non-landmark (Lines 2 to 5). If a neighbor, v , is a landmark (Line 6), we set v to represent the current data point (Lines 7 and 8). If v is not a landmark but is associated with one (Line 9), the landmark that represents v will also represent the current data point (Lines 10 and 11). Finally, we begin a depth-first search in the k -nearest

Algorithm 1 Associate Landmarks.

```

1: procedure ASSOCIATE_LANDMARK( $X$ )
2:   for  $u \in X$  do
3:     if not landmark( $u$ ) then
4:       found  $\leftarrow$  false
5:       for  $v \in NH(u)$  do
6:         if landmark( $v$ ) then
7:           found  $\leftarrow$  true
8:           associate[ $u$ ]  $\leftarrow$   $v$ 
9:         else if associate[ $v$ ]  $\neq$  NIL then
10:          found  $\leftarrow$  true
11:          associate[ $u$ ]  $\leftarrow$  associate[ $v$ ]
12:       if not found then
13:         landmark  $\leftarrow$  depth-first search on graph  $X$  starting in  $u$ 
14:         associate[ $u$ ]  $\leftarrow$  landmark

```

neighbor graph and associate the first landmark found with the current data point if neither of these scenarios holds true for all neighborhoods.

With the data points assigned to each landmark, users can select a list of indices on level H^i to embed the associated data points on H^{i-1} . Thus, supposing the list of indices in H^i is denoted by I , we only have to create the matrix $p_{mn}^{i-1} = \{p_{mn} \mid A[m] \in I \wedge A[n] \in I\}$, where $A[u]$ returns the landmark that represents the data point x_u .

3.3.2 Mental map preservation

When modifications are made to the initial visualization through updates on the current dataset at time t , the concept of mental map preservation entails maintaining the same overall layout shape and point positioning [2, 10]. These updates may involve new data points or modifications to the features of existing data points; in the case of interacting with hierarchical dimensionality reduction results, the new data points are drawn from lower hierarchy levels.

The subsets of data chosen for fine-grained exploration on level l during hierarchical exploration must resemble the organization of level $l-1$, especially for unlabeled datasets. Rauber et al. [37] and Fujiwara et al. [37] also present strategies to deal with mental map preservation in the context of dimensionality reduction, even though the majority of the work on mental map preservation is limited to dynamic graph drawing [23, 48]. In both situations, the goal is to ease the analysis burden during exploration and facilitate smoother embedding layout changes. Fig. 3 shows successive hierarchical projections using HUMAP, whether or not the mental map is preserved. Note that it is difficult to track the data transformations if mental maps are not preserved.

HUMAP uses the coordinates of higher—and already projected—data points on level l to guide the positioning of level $l-1$. When initializing the low-dimensional representation before Stochastic Gradient Descent (SGD) optimization, the coordinates for the projected data points in l are used as starting points together with the remaining data points initialized with Spectral Embedding—these coordinates only move a fraction during SGD optimization. Thus, we also provide this fraction hyperparameter θ to be tuned according to one's needs, although we empirically find that $\theta = 0.01$ yields embeddings that best preserve the mental map throughout the hierarchy expansion.

4 CASE STUDIES

In this section, we provide two case studies. In the first, we leverage a dimensionality reduction explanation approach to show how HUMAP benefits the analysis in terms of the various facets that a hierarchical dimensionality reduction can offer. Then, we attest HUMAP's performance regarding mental map preservation when dealing with a big dataset. For both case studies, we set the number of random walks $\omega = 20$ and the length of each random walk $v = 30$.

4.1 Exploring CNN's learned features

In this case study, we explore the learned features of a convolutional neural network (CNN). Here, we aim to emphasize mental map preservation across hierarchy levels, which is beneficial when exploring a

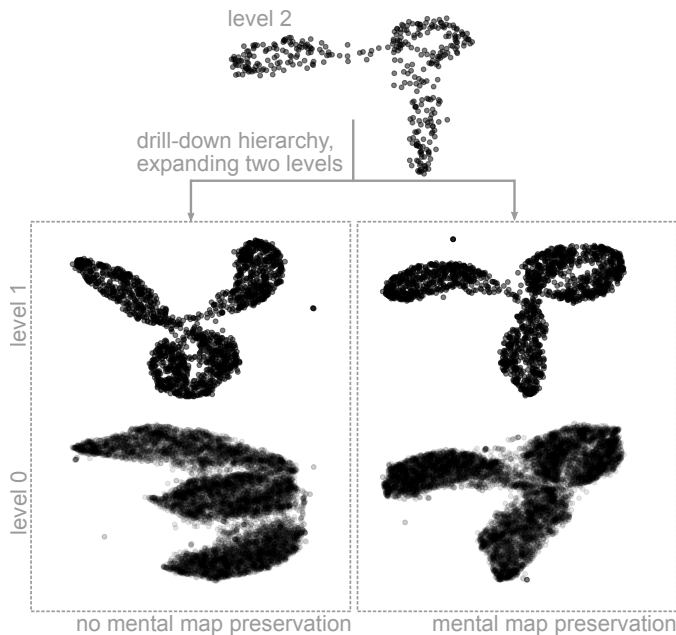


Fig. 3: Hierarchical exploration with HUMAP using mental map.

large number of data points. We used the Fashion MNIST dataset [47], composed of 70,000 of 28×28 grayscale images of fashion items (clothing, footwear, and bags). Our architecture consists of $32 \times 3 \times 3$ convolutional filters, $64 \times 3 \times 3$ convolutional filters, a dense layer of 128 neurons, and a softmax layer of ten neurons. We used the dense layer as features for each image after training the dataset, resulting in a $70,000 \times 128$ matrix. Fig. 4(A) shows the top level of HUMAP created using three hierarchy levels. Each data point is color-coded using its ground truth labels, where the gray border encodes misclassification by the CNN. Notice the four main clusters, where three of them we further explore by selecting data points for drilling down the hierarchy, as indicated by the arrows.

We start by analyzing the separation of cluster \bullet in the projection. The subsequent level of the hierarchy (see Fig. 4(B)) and the images representing a few data samples show that the features learned by the CNN can differentiate purses with and without visible handles. The explanation computed using SHAP [24] shows how each part of the image contributes to augmenting (in blue) or decreasing (in red) the prediction probability for each class. Based on SHAP analysis, having a visible shoulder strap is very determinant in assigning a data sample in the bag group. If a bag does not have this item, its rectangular format contributes to the correct classification.

Then, for the cluster highlighted in purple in Fig. 4(A), we investigate the misclassification of data samples by projecting another hierarchy level (C). The selection of data samples from \bullet and \bullet in Fig. 4(C) show that the CNN confusion of classifying sneakers as high-heels was due to image intensity. For the instance explained using SHAP, the CNN assigned too much importance to the middle part of the sneakers, augmenting the probability for class \bullet . The sneaker has darker colors, a characteristic that CNN learned to recognize high-heels. Then, we project the last hierarchy level (Fig. 4(D)) to investigate the group of boots (\bullet). Inspecting the explanations for two data samples, the sample of class \bullet was apparently misclassified by the fact that it does not present protection (or darker color in the image) on the ankle area—see this aspect on SHAP values for classes \bullet and \bullet .

Finally, we drill down to the second level using the data samples from the cluster highlighted in green in Fig. 4(A), resulting in Fig. 4(E). Then, we proceed to the lowest level of the hierarchy by selecting another cluster (Fig. 4(F)). The cluster correspond to dresses \bullet , t-shirts \bullet , and a smaller number of samples from coats \bullet . Focusing on CNN’s misclassifications, we see several samples from class \bullet that do not have

sleeves (tank tops and blouses), making the CNN misclassify them with dresses. The SHAP explanations show that the highlighted tank top was misclassified as a dress (class \bullet) since CNN focused on the absence of sleeves.

5 NUMERICAL EVALUATION

In this section, we numerically evaluate HUMAP² and compare it against existing HDR techniques. We compare our approach with Hierarchical Stochastic Neighbor Embedding (HSNE)³ [35], Multiscale PHATE⁴ [21], and UMAP⁵ [28] by using their official implementation. We cannot control the number of data points in each hierarchy level in HSNE and Multiscale PHATE. Thus, we generate HSNE with three levels and a HUMAP hierarchy with three levels based on the number of data points in each HSNE level. Multiscale PHATE does not accept a parameter to specify the number of levels. After fitting the Multiscale PHATE hierarchy, we search for a level with a size similar to the top-level produced by HUMAP and HSNE techniques. Finally, we evaluate UMAP to demonstrate its differences from HUMAP regarding mental map and structure preservation. Thus, to simulate hierarchy levels using UMAP, we project the same data points generated in the HUMAP hierarchy.

We use the following datasets for evaluation. MNIST [22] is a dataset composed of 70,000 28×28 pixel grayscale images of handwritten digits classified into ten classes (from 0 to 9), where each flattened image results in a 784 dimensional vector. Fashion MNIST [47] (FMNIST) is a dataset composed of 70,000 28×28 pixel grayscale images of fashion items (clothing, footwear, and bags) divided into ten classes; each flattened image results in a 784 dimensional vector. Mammals is a synthetic dataset designed to have four well-separated classes, and it consists of 20,000 data points described by 72 dimensions. Embryoid Body (EB) is a single-cell RNA sequencing dataset for embryoid body data generated over 27 days [30] divided into five periods. For this dataset, we aim to visualize the development of the 31,000 cells after preprocessing them and using the first 50 principal components to perform the projections. Note that, FMNIST, MNIST, and Mammals datasets are meant to produce cohesive clusters after embedding, while the ideal result for Embryoid Body is to provide an understanding of its continuous structures—this is an attempt to understand how HUMAP compares to different techniques regarding their most known characteristics, that is, to cluster data (HSNE, derived from SNE) and to emphasize continuity (Multiscale PHATE derived from PHATE). The experiments were performed in a computer with the following configuration: Intel(R) Core(TM) i7-8700 CPU @ 3.20 GHz, 32 GB RAM, Ubuntu 64 bits, NVIDIA GeForce GTX 1660 Ti 22 GB.

Dataset	Size	Dimensions
Mammals	20000	72
Embryoid Body (EB)	31000	17845 \rightarrow PCA(50)
MNIST	70000	784
FMNIST	70000	784

Table 1: Datasets used for experimentation.

Fig. 5 depicts the embeddings for the hierarchy levels. For few datasets, the HSNE method does not preserve the top-level structure. Although the top-level embedding shows a good relationship between clusters, it embeds clusters too closely together for the projection of the entire datasets, as seen, for instance, in the clusters for the mammals dataset on level 0. The continuous nature of the biological data is not shown for the EB dataset. One significant problem, to sum up, is that the mental map cannot be maintained throughout the hierarchy.

Due to their high dimensionality, Multiscale PHATE was unable to produce embeddings for the FMNIST and MNIST datasets. Despite

²<https://github.com/wilsonjr/humap>

³<https://github.com/biovault/nptsne>

⁴https://github.com/KrishnaswamyLab/Multiscale_PHATE

⁵<https://github.com/lmcinnes/umap>

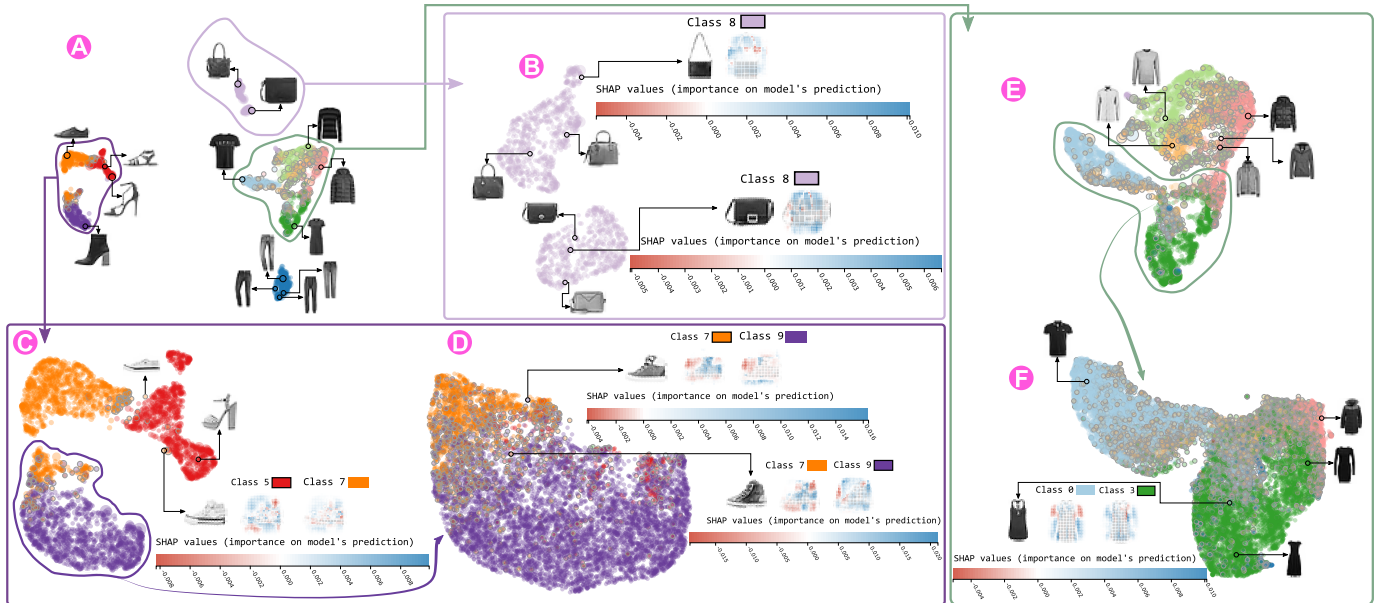


Fig. 4: Hierarchical exploration of the learning weights and explanations of a CNN trained on Fashion MNIST dataset. The top hierarchy level (A) encodes the overview of the dataset. Exploring lower levels by drilling-down the hierarchy (B-F) reveals more detailed information while preserving the mental map.

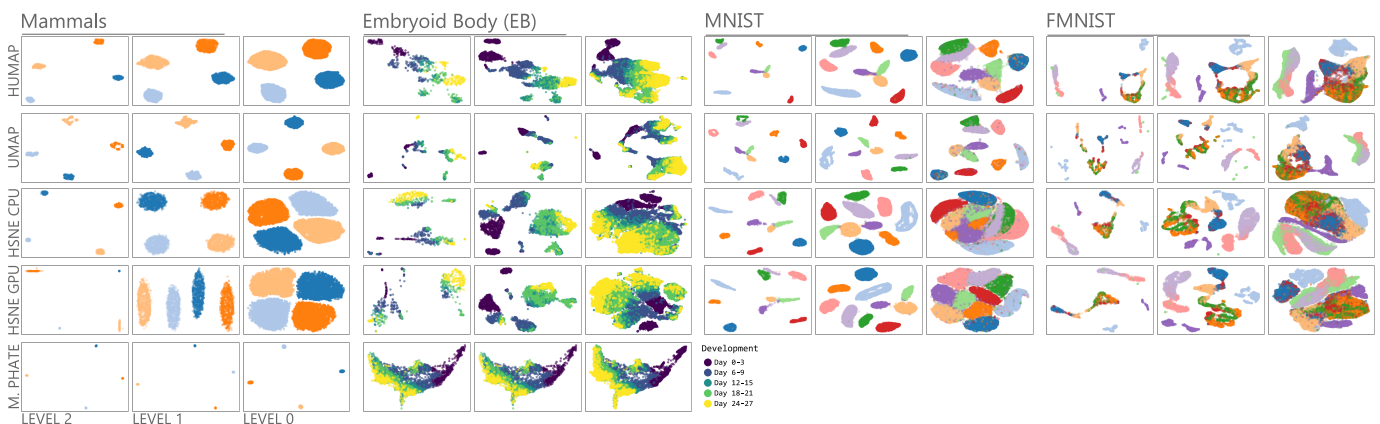


Fig. 5: Visual analysis of the embeddings generated for top and lowest hierarchical levels using a three-level hierarchy. For each dataset, top-level embedding appears on the left, and the lowest level (whole dataset) appears on the right.

revealing the continuous nature of the EB dataset, it produced embeddings for the mammals dataset that made analysis challenging because the data points for each cluster were too close to one another. On the other hand, HUMAP maintains the mental map through all levels of the hierarchy by encoding the data from lower levels at higher levels. The main challenge for Multiscale PHATE appears to be shrinking high-dimensional datasets without doing so in a tractable manner (e.g., by using PCA). This has more to do with computational power than it does with Multiscale PHATE's accuracy in recognizing structures and similarity relationships.

Finally, UMAP only reveals the correct overview for the simpler datasets on level 2. (e.g., *mammals* and *MNIST*). UMAP is unable to uncover the structures displayed at the lowest level for the *EB* and *FMNIST* datasets. This outcome was anticipated because UMAP's primary objective is not to transfer the relationship between data points to the projection sample. The ability to successfully encode datasets with less data is achieved by HUMAP, which projects higher levels based on relationships at lower levels.

For the numerical evaluation, we compare the techniques using well-known and traditional quality metrics for embedding evaluation (e.g., *Trustworthiness* and *Continuity* in **Supplementary File**) as well

as the metrics that appear in the related works, such as *DeMaP* [29] and *Neighborhood Preservation* [34] that aim to evaluate how the low-dimensional embeddings represent the structures in higher dimensions.

5.1 Running-time

Due to the stochastic nature of these techniques, we run the experiments twenty times for each evaluation metric while adhering to the steps outlined at the beginning of this section. In order to fit the hierarchy and embed levels 2 and 0, Fig. 6 displays boxen-plots in log scale for runtime execution (seconds) (the whole dataset). Humap offers comparable runtime execution to HSNE in GPU, with the exception of level 0, making it a promising strategy for users with limited resources when reasonable runtime execution is required. When fitting the hierarchy, HUMAP takes slightly longer than HSNE to run on the CPU, but it is quicker when embedding the hierarchy levels. When many data points are embedded, multiscale PHATE seems unreasonable for interactive applications (for example, level 0 of mammals and EB datasets). Finally, as we approach the lowest level, the difference between HUMAP and UMAP narrows due to their increasing sizes.

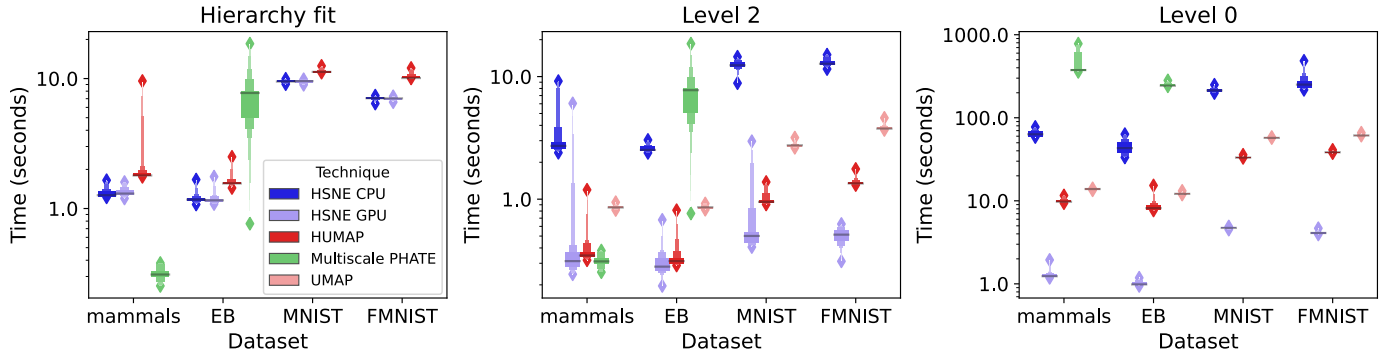


Fig. 6: Runtime execution in seconds using a \log_{10} scale. The boxen-plots show the runtime for 20 runs of each technique under the same condition—we measure the runtime to fit the hierarchy (Hierarchy fit), to embed the top level (Level 2), and to embed the whole dataset (Level 0).

5.2 Neighborhood Preservation

Fig. 7 depicts the neighborhood preservation (NP) for a variable number of neighbors, k ($k \in [1, 30]$). Such a metric calculates the mean ratio of neighbors preserved in the projection. When using datasets for other analyses, or when the main objective is to identify global relationships among clusters rather than just concentrating on local structures, the HUMAP technique reveals lower neighborhood preservation.

The *mammals* dataset is intended to have clearly defined classes, whereas the *EB* dataset is intended for continuity analysis. Because it does not just concentrate on local structures when projecting such datasets, HUMAP achieves a lower NP. The characteristics of SNE are inherited by HSNE, which exhibits a higher NP for cluster separation (see the *EB* projections, for example).

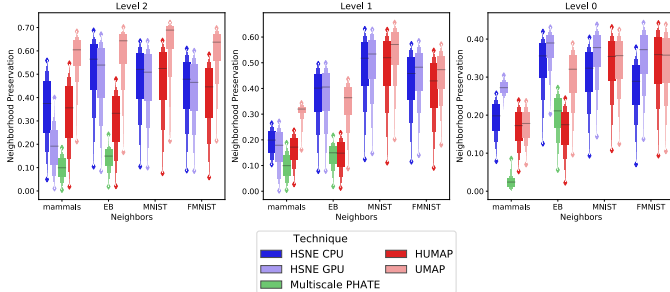


Fig. 7: Neighborhood Preservation after embedding on \mathbb{R}^2 . HSNE outperforms HUMAP by a great margin only for *EB* dataset.

We evaluated HUMAP using various values of β (which controls the local neighbors’ contribution to the similarity among landmarks), and the results clearly demonstrated the link between local neighborhoods and neighborhood preservation. In addition, for the MNIST dataset at the top hierarchy levels, HUMAP outperforms HSNE by a considerable margin with the addition of only 3% of the current neighborhood (100 neighbors). Similar data points are visually grouped together by HUMAP as a result of the β parameter; interested readers can visualize the analyses and projections for this scenario in the **Supplementary File** (Figs. 3 and 4).

5.3 DEMaP

We employ the DEMaP metric [29], which calculates the Spearman correlation between geodesic distances on high-dimensional and euclidean distances on low-dimensions, to assess how well the techniques convey manifolds, clusters, and other high-dimensional space structures. On level 2, HUMAP outperformed HSNE, UMAP, and GPU-based HSNE for the MNIST and FMNIST datasets, as shown in Fig. 8. The pair of distributions (HUMAP, UMAP) for the *EB*, *FMNIST* datasets on level 2 and for the *EB* dataset on level 0 are not statistically different after a t-test, but the others are with a p-value of at least 0.00001 (see **Supplementary File** - Table 2 for the details). When the entire dataset

is embedded for the *mammals* dataset, HUMAP displays higher values, providing proof that our method is stable across hierarchical levels. While HSNE and Multiscale PHATE produce better results at the top of the hierarchy, they omit key details as one descends hierarchy. The relationship among clusters is lost on the HSNE side. Finally, as shown by its DEMaP values, HUMAP conveys the continuous structures present in the *EB* dataset even for the top-level embedding. However, Multiscale PHATE and HSNE on the CPU show higher DEMaP values at level 0.

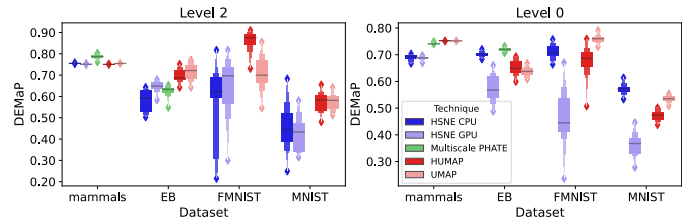


Fig. 8: Evaluation of techniques’ ability to represent complex structures such as clusters, manifolds, and other relationships.

Although HUMAP shows lower DEMaP values for *mammals* on the top-level and *EB* on level 0, Fig. 5 demonstrates the mental map preservation across hierarchical levels. In particular for unlabelled datasets, the preservation of the mental map is crucial to avoid misleading users and increasing cognitive load during exploration; this characteristic also holds for subsets of data points, which we address in the following section. According to the DEMaP metric, the fixing term for maintaining the mental map lowers the quality of the entire projection (level 0). We restrict the flexibility of the optimization algorithm when positioning the data points when we set the embedding of lower hierarchy levels to follow the pattern of higher hierarchy levels. In the **Supplementary File** (Section 5), we provide the same analysis by setting free the optimization algorithm ($\theta = 1$), which results in higher DEMaP values.

5.4 Projecting subsets of data

In this section, the methods are contrasted according to how well they can project subsets of data points. Since there is no way to drill down a hierarchy based on classes of data points, we do not analyze Multiscale PHATE. The dimensionality of MNIST and FMNIST could be handled by Multiscale PHATE. Fig. 9a illustrates the same pattern as Fig. 5, in which HUMAP conveys top-level structures and maintains the mental map throughout the hierarchy. In this case, we project a four-level hierarchy, adding complexity to the analysis. In Fig. 9a, the first level’s subset was lasso-selected, and the subsequent levels’ subsets were chosen according to specific classes.

In all scenarios, as shown in Fig. 9b, HUMAP has a higher DEMaP than HSNE, and it only falls short of UMAP on the fourth level for the MNIST dataset—notice that UMAP by itself does not take the relation-

ship between higher levels into account for projection. Additionally, Fig. 9b (a) shows how crucial mental map preservation is when users want to invert more of the embedding.

5.5 Other quantitative evaluations

After dimensionality reduction, additional quality metrics can be used to assess the final embedding (e.g., *Trustworthiness*, *Continuity*). In order to broaden the analysis performed in this paper, another set of comparisons are presented in the **Supplementary File**. In the *Runtime* analysis, we carefully examine how each HUMAP step is impacted by the dataset size and dimensionality as well as how it compares against the alternatives. We demonstrate in the *Reproducibility* analysis that HUMAP can be just as effective as UMAP in terms of the reproducibility of subsequent runs. Finally, we also performed a parameter analysis to comprehend HUMAP's behavior for various parameter configurations.

6 DISCUSSIONS

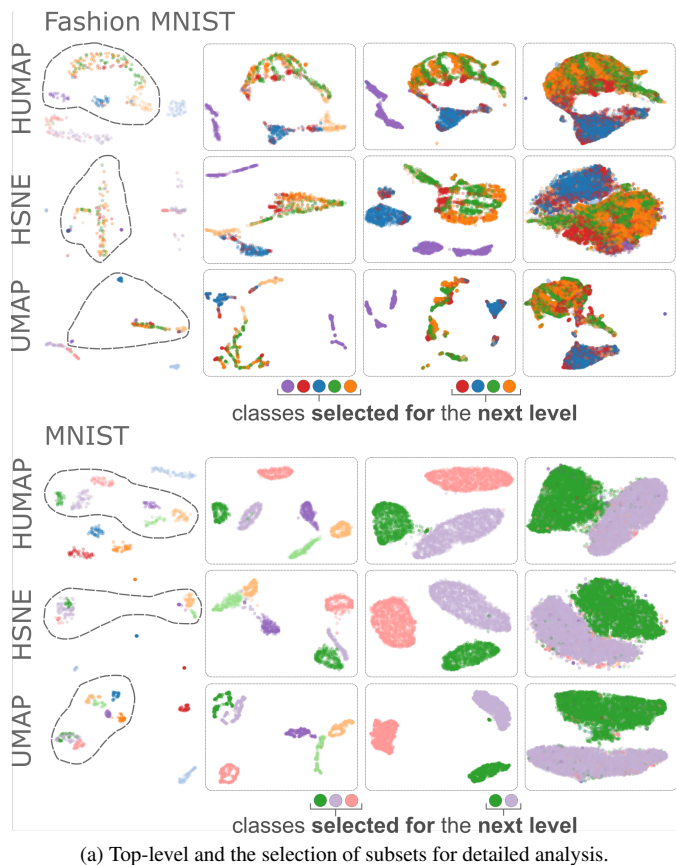
The experiments demonstrate that HUMAP is competitive with GPU-based methods in terms of running time execution while outperforming current approaches in their ability to represent structures found in high-dimensional spaces. It also preserves the relationships among data clusters and other structures at various levels of the hierarchy, which is an important factor. Since HUMAP preserves the overall structures of higher hierarchy levels at lower hierarchy levels, it is an ideal tool for progressive analysis [9]. Here, we go over a few of the features of our method.

Reproducibility. At the expense of a longer run-time execution, HUMAP allows for the generation of reproducible embeddings. In other words, we need to disable a few parallel execution steps in the components for hierarchical definition and projection. When we measure the correlation of data points across successive projections [3], experiments demonstrate perfect reproducibility for HUMAP for various datasets. This makes it possible to collaborate on difficult or time-consuming tasks, as the one exemplified in the case study.

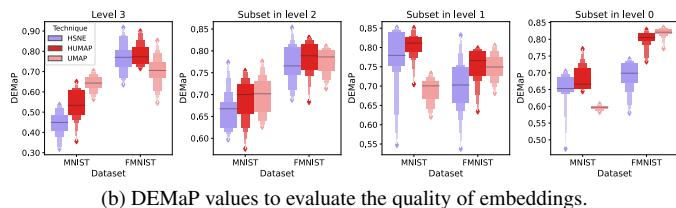
Embedding initialization and CPU/GPU implementations. Recent research demonstrates that the initialization of the low-dimensional representation significantly affects the performance of these two algorithms, with PCA [18] being preferable to random initialization for t-SNE [19]. T-SNE with random initialization is used in HSNE. This fact may help to explain why the HSNE yielded lower results for DEMaP metric at the lowest level (the entire dataset). However, HSNE effectively encodes the global neighborhood at higher hierarchy levels, so we believe integrating this initialization step would still not impact the final results. The embedding cannot currently be started with PCA initialization using the official HSNE implementation. PCA initialization, however, does not address the issue of the mental map not being preserved across hierarchy levels.

The performance of HSNE on the CPU being consistently superior to HSNE on the GPU is another intriguing aspect of the numerical comparison. But why do we observe such a contrast? First, the embeddings are computed by HSNE on GPU using the GPGPU approximation. Although it produces acceptable embeddings, this approximation compromises accuracy for runtime. The Barnes-Hut implementation is used by HSNE on the CPU to compute the embeddings with $\theta=0$, the speed/accuracy trade-off parameter, which ranges from 0 (exact t-SNE) to 1 (approximated t-SNE).

Landmark selection. We must choose representative data points (or landmarks) to be a subset of the dataset for a specific hierarchy level in order to define different hierarchy levels. For this task, we empirically assessed a number of strategies. Only evenly distributed datasets can benefit from choosing landmarks from denser neighborhoods; otherwise, hierarchy levels might only be able to encode some of the data (the dense regions). The soft-max of σ_i , for example, produces too many data points on non-dense regions when a probability vector is created using density information. Finally, because of the computational complexity and difficulty in accurately capturing the data organization



(a) Top-level and the selection of subsets for detailed analysis.



(b) DEMaP values to evaluate the quality of embeddings.

Fig. 9: Using HUMAP, UMAP, and HSNE to project a subset of data.

given outliers and other data structures, such as clusters of different shapes, clustering approaches do not work well for our problem.

HUMAP generalizability and scalability. In order to show the efficacy of HUMAP for hierarchical exploration, we contrasted it with various hierarchical dimensionality reduction methods, as well as with UMAP, throughout the experiments. We also provided case studies that explored datasets with various characteristics using HUMAP. Despite the fact that we are aware that different hyperparameters might produce varying results, we use the techniques' default parameters in this context to provide the analysis. We attempted to track various applications for a dimensionality reduction technique, from comprehending clusters for multidimensional datasets to visualizing single-cell sequencing data, although a more thorough study would be an interesting topic for future research activities. In the **Supplemental File** that is included, we also provide a comprehensive examination of HUMAP's scalability and generalizability.

7 CONCLUSION

For the analysis of high-dimensional data, DR techniques are excellent tools. Traditional methods, however, are unable to reveal substructures while giving a dataset's overview. Hierarchical DR approaches offer analysis that adheres to the mantra of visualization, in which analysts concentrate on crucial information and retain details as needed, in order to mitigate this problem. However, the hierarchical approaches described in the literature either cannot be applied to a wide range of dataset types or do not preserve the mental map throughout the hierarchy levels.

We introduce HUMAP, a novel hierarchical DR technique, in this paper. It provides a viable alternative to high-dimensional data analysis because it addresses issues that current methods do not adequately address. HUMAP offers tunable parameters that make it simple to concentrate on global or local neighborhood preservation in addition to maintaining the mental map and global and local relationships.

Future research will expand on our technique to examine distance metrics between landmarks and data points. Additionally, we intend to implement GPU versions to enable users to delve deeper into HUMAP's capabilities. Finally, we intend to conduct user experiments on the significance of mental map preservation for hierarchical approaches and investigate novel strategies to evaluate hierarchical DR techniques.

ACKNOWLEDGMENTS

This work was supported by Fundação de Amparo à Pesquisa (FAPESP) [grant number #2018/17881-3] and the Coordenação de Aperfeiçoamento de Pessoal de Nível Superior (CAPES) [grant number #88887.487331/2020-00].

REFERENCES

- [1] A. Agarwal, T. El-Ghazawi, H. El-Askary, and J. Le-Moigne. Efficient hierarchical-pca dimension reduction for hyperspectral imagery. In *2007 IEEE International Symposium on Signal Processing and Information Technology*, pp. 353–356, 2007. doi: 10.1109/ISSPIT.2007.4458191
- [2] D. W. Archambault, H. C. Purchase, and B. Pinaud. Animation, small multiples, and the effect of mental map preservation in dynamic graphs. *IEEE Transactions on Visualization and Computer Graphics*, 17:539–552, 2011.
- [3] E. Becht, L. McInnes, J. Healy, C.-A. Dutertre, I. Kwok, L. G. Ng, F. Ginhoux, and E. W. Newell. Dimensionality reduction for visualizing single-cell data using umap. *Nature Biotechnology*, 37:38–44, 2018.
- [4] B. C. Benato, A. C. Telea, and A. X. Falcão. Semi-supervised learning with interactive label propagation guided by feature space projections. In *2018 31st SIBGRAPI Conference on Graphics, Patterns and Images (SIBGRAPI)*, pp. 392–399, 2018. doi: 10.1109/SIBGRAPI.2018.00057
- [5] N. Brugnone, A. Gonopolskiy, M. W. Moyle, M. Kuchroo, D. V. Dijk, K. R. Moon, D. A. Colón-Ramos, G. Wolf, M. J. Hirn, and S. Krishnaswamy. Coarse graining of data via inhomogeneous diffusion condensation. *2019 IEEE International Conference on Big Data (Big Data)*, pp. 2624–2633, 2019.

- [6] G. D. Cantareira and F. V. Paulovich. A Generic Model for Projection Alignment Applied to Neural Network Visualization. In C. Turkyay and K. Vrotsou, eds., *EuroVis Workshop on Visual Analytics (EuroVA)*. The Eurographics Association, 2020. doi: 10.2312/eurova.20201089
- [7] D. M. Eler, F. V. Paulovich, M. C. F. d. Oliveira, and R. Minghim. Topic-based coordination for visual analysis of evolving document collections. In *2009 13th International Conference Information Visualisation*, pp. 149–155, 2009. doi: 10.1109/IV.2009.31
- [8] M. Espadoto, R. M. Martins, A. Kerren, N. S. T. Hirata, and A. C. Telea. Towards a quantitative survey of dimension reduction techniques. *IEEE Transactions on Visualization and Computer Graphics*, pp. 1–1, 2019. doi: 10.1109/TVCG.2019.2944182
- [9] T. Fujiwara, J.-K. Chou, Shilpika, P. Xu, L. Ren, and K.-L. Ma. An incremental dimensionality reduction method for visualizing streaming multidimensional data. *IEEE Transactions on Visualization and Computer Graphics*, 26:418–428, 2020.
- [10] T. Fujiwara, O.-H. Kwon, and K.-L. Ma. Supporting analysis of dimensionality reduction results with contrastive learning. *IEEE Trans. Vis. and Comp. Graph.*, 26:45–55, 2019.
- [11] C. Geyer. *Introduction to markov chain monte carlo*. 2011.
- [12] G. M. Hilasaca and F. V. Paulovich. Visual feature fusion and its application to support unsupervised clustering tasks. *Information Visualization*, 19(2):163–179, 2020.
- [13] T. Höllt, A. Vilanova, N. Pezzotti, B. Lelieveldt, and H. Hauser. Focus+context exploration of hierarchical embeddings. *Computer Graphics Forum (Proceedings of EuroVis 2019)*, (3), 2019. doi: 10.1111/cgf.13711
- [14] T. Höllt, N. Pezzotti, V. van Unen, F. Koning, B. P. F. Lelieveldt, and A. Vilanova. Cyteguide: Visual guidance for hierarchical single-cell analysis. *IEEE Transactions on Visualization and Computer Graphics*, 24(1):739–748, 2018.
- [15] S. Ingram, T. Munzner, and M. Olano. Glimmer: Multilevel mds on the gpu. *IEEE Transactions on Visualization and Computer Graphics*, 15:249–261, 2009.
- [16] K. Janné, J. Pettersen, N.-O. Lindberg, and T. Lundstedt. Hierarchical principal component analysis (pca) and projection to latent structure (pls) technique on spectroscopic data as a data pretreatment for calibration. *Journal of Chemometrics*, 15(4):203–213, 2001.
- [17] P. Joia, D. Coimbra, J. A. Cuminato, F. V. Paulovich, and L. G. Nonato. Local affine multidimensional projection. *IEEE Transactions on Visualization and Computer Graphics*, 17(12):2563–2571, 2011. doi: 10.1109/TVCG.2011.220
- [18] I. Jolliffe. *Principal Component Analysis*. Springer Verlag, 1986.
- [19] D. Kobak and G. C. Linderman. Initialization is critical for preserving global data structure in both t-sne and umap. *Nature biotechnology*, 2021.
- [20] R. Krueger, J. Beyer, W. Jang, N. W. Kim, A. Sokolov, P. K. Sorger, and H. Pfister. Facetto: Combining unsupervised and supervised learning for hierarchical phenotype analysis in multi-channel image data. *IEEE Transactions on Visualization and Computer Graphics*, 26(1):227–237, 2020.
- [21] M. e. a. Kuchroo. Multiscale phate exploration of sars-cov-2 data reveals multimodal signatures of disease. *bioRxiv*, 2020. doi: 10.1101/2020.11.15.383661
- [22] Y. LeCun and C. Cortes. MNIST handwritten digit database. 2010.
- [23] L. Leydesdorff and T. Schank. Dynamic animations of journal maps: Indicators of structural changes and interdisciplinary developments. 59(11):1810–1818, sep 2008.
- [24] S. M. Lundberg and S.-I. Lee. A unified approach to interpreting model predictions. In I. Guyon, U. V. Luxburg, S. Bengio, H. Wallach, R. Fergus, S. Vishwanathan, and R. Garnett, eds., *Advances in Neural Information Processing Systems 30*, pp. 4765–4774. Curran Associates, Inc., 2017.
- [25] D. Lähnemann, J. Köster, and E. e. a. Szczurek. Eleven grand challenges in single-cell data science. *Genome Biol*, 31, 2020.
- [26] L. V. D. Maaten and G. E. Hinton. Visualizing data using t-sne. *Journal of Machine Learning Research*, 9:2579–2605, 2008.
- [27] W. E. Marcilio-Jr, D. M. Eler, R. E. Garcia, R. C. M. Correia, and L. F. Silva. A hybrid visualization approach to perform analysis of feature spaces. In S. Latifi, ed., *17th International Conference on Information Technology—New Generations (ITNG 2020)*, pp. 241–247. Springer International Publishing, Cham, 2020.
- [28] L. McInnes and J. Healy. Umap: Uniform manifold approximation and projection for dimension reduction. *ArXiv*, abs/1802.03426, 2018.
- [29] K. Moon, D. van Dijk, and Z. e. a. Wang. Visualizing structure and transitions in high-dimensional biological data. *Nat Biotechnol*, pp. 1482–

1492, 2019. doi: 10.1038/s41587-019-0336-3

- [30] Moon, Keving. Embryoid body data for phate. <https://data.mendeley.com/datasets/v6n743h5ng/1>, 2018. Online; accessed 02 February 2021. doi: 10.17632/v6n743h5ng.1
- [31] A. Y. Ng, M. I. Jordan, and Y. Weiss. On spectral clustering: Analysis and an algorithm. In *ADVANCES IN NEURAL INFORMATION PROCESSING SYSTEMS*, pp. 849–856. MIT Press, 2001.
- [32] L. G. Nonato and M. Aupetit. Multidimensional projection for visual analytics: Linking techniques with distortions, tasks, and layout enrichment. *IEEE Transactions on Visualization and Computer Graphics*, 25(8):2650–2673, 2019. doi: 10.1109/TVCG.2018.2846735
- [33] F. V. Paulovich and R. Minghim. Hipp: A novel hierarchical point placement strategy and its application to the exploration of document collections. *IEEE Transactions on Visualization and Computer Graphics*, 14(6):1229–1236, 2008. doi: 10.1109/TVCG.2008.138
- [34] F. V. Paulovich, L. G. Nonato, R. Minghim, and H. Levkowitz. Least square projection: A fast high-precision multidimensional projection technique and its application to document mapping. *IEEE Transactions on Visualization and Computer Graphics*, 14(3):564–575, 2008. doi: 10.1109/TVCG.2007.70443
- [35] N. Pezzotti, T. Höllt, B. Lelieveldt, E. Eisemann, and A. Vilanova. Hierarchical stochastic neighbor embedding. *Computer Graphics Forum*, 35(3):21–30, 2016. doi: 10.1111/cgf.12878
- [36] P. E. Rauber, S. G. Fadel, A. X. Falcão, and A. C. Telea. Visualizing the hidden activity of artificial neural networks. *IEEE Transactions on Visualization and Computer Graphics*, 23(1):101–110, 2017. doi: 10.1109/TVCG.2016.2598838
- [37] P. E. Rauber, A. X. Falcão, and A. C. Telea. Visualizing time-dependent data using dynamic t-sne. EuroVis '16, p. 73–77. Eurographics Association, Goslar, DEU, 2016.
- [38] S. Ruder. An overview of gradient descent optimization algorithms. *ArXiv*, abs/1609.04747, 2016.
- [39] J. Salamon, X. Qian, M. Nilsson, and D. J. Lynn. Network visualization and analysis of spatially aware gene expression data with insitunet. *Cell systems*, 6 5:626–630.e3, 2018.
- [40] A. Sarikaya and M. Gleicher. Scatterplots: Tasks, data, and designs. *IEEE Transactions on Visualization and Computer Graphics*, 24(1):402–412, 2018. doi: 10.1109/TVCG.2017.2744184
- [41] M. Sedlmair, T. Munzner, and M. Tory. Empirical guidance on scatterplot and dimension reduction technique choices. *IEEE Transactions on Visualization and Computer Graphics*, 19(12):2634–2643, 2013. doi: 10.1109/TVCG.2013.153
- [42] B. Shneiderman. The eyes have it: a task by data type taxonomy for information visualizations. In *Proceedings 1996 IEEE Symposium on Visual Languages*, pp. 336–343, 1996. doi: 10.1109/VL.1996.545307
- [43] A. Somarakis, V. van Unen, F. Koning, B. P. F. Lelieveldt, and T. Hollt. Imacyte: Visual exploration of cellular microenvironments for imaging mass cytometry data. *IEEE transactions on visualization and computer graphics*, 2019.
- [44] V. van Unen, T. Höllt, N. Pezzotti, N. Li, M. Reinders, E. Eisemann, A. Vilanova, F. Koning, and B. Lelieveldt. Visual analysis of mass cytometry data by hierarchical stochastic neighbor embedding reveals rare cell types. *Nature Communications*, 8(1740):1 – 10, 2017. doi: 10.1038/s41467-017-01689-9
- [45] J. A. Westerhuis, T. Kourti, and J. F. MacGregor. Analysis of multiblock and hierarchical pca and pls models. *Journal of Chemometrics*, 12(5):301–321, 1998.
- [46] M. Williams and T. Munzner. Steerable, progressive multidimensional scaling. In *IEEE Symposium on Information Visualization*, pp. 57–64, 2004. doi: 10.1109/INFVIS.2004.60
- [47] H. Xiao, K. Rasul, and R. Vollgraf. Fashion-mnist: a novel image dataset for benchmarking machine learning algorithms. *ArXiv*, abs/1708.07747, 2017.
- [48] K. S. Xu, M. Klinger, and A. O. Hero. A regularized graph layout framework for dynamic network visualization. *Data Mining and Knowledge Discovery*, 27:84–116, 2012.